

Superparamagnetism versus superspin glass behavior in dilute magnetic nanoparticle systems

Xi Chen,^{1,*} S. Bedanta,¹ O. Petracic,¹ W. Kleemann,¹ S. Sahoo,^{1,2} S. Cardoso,³ and P. P. Freitas³

¹*Angewandte Physik, Universität Duisburg-Essen, D-47048 Duisburg, Germany*

²*Behlen Laboratory of Physics, Department of Physics and Astronomy, University of Nebraska, Lincoln, Nebraska 68588-0111, USA*

³*INESC, Rua Alves Redol 9-1, 1000 Lisbon, Portugal*

(Received 10 May 2005; revised manuscript received 7 November 2005; published 28 December 2005)

The magnetization of diluted nanoparticle systems $[\text{Co}_{80}\text{Fe}_{20}(t_n)/\text{Al}_2\text{O}_3(3\text{ nm})]_{10}$ with $t_n=0.7$ and 0.5 nm reveals strong paramagnetic contributions at low temperatures. They are due to atomically small magnetic clusters, which are undetectable in transmission electron microscopy and surround nanoparticles with saturating field-cooled magnetization. Zero field memory effects unequivocally discriminate between superspin glass and superparamagnetic behavior for $t_n=0.7$ and 0.5 nm, respectively.

DOI: [10.1103/PhysRevB.72.214436](https://doi.org/10.1103/PhysRevB.72.214436)

PACS number(s): 75.20.-g, 75.40.Gb, 75.50.Lk, 75.50.Tt

Since the pioneering work of Néel five decades ago,¹ the magnetic properties of nanoparticles have gained high interest from both technological and fundamental research. In an isolated noninteracting single domain particle (superspin) system, the simplest model due to Néel and Brown^{1,2} predicts superparamagnetic (SPM) behavior and magnetization blocking at high and low temperatures T , respectively. At finite interparticle distances, more complicated systems are encountered due to magnetic interactions, especially of dipolar origin. With the increase of the interaction strength, modified SPM behavior,³⁻⁵ superspin glass (SSG),⁴⁻⁹ and superferromagnetic (SFM) states^{7,10,11} appear sequentially.

Recently a magnetic phase diagram¹² was presented for a nearly ideal model system consisting of discontinuous $[\text{Co}_{80}\text{Fe}_{20}(t_n)/\text{Al}_2\text{O}_3(3\text{ nm})]_{10}$ multilayers, where the nominal thickness t_n is related to the nanoparticle concentration. Below the physical percolation threshold, $t_n=1.8$ nm,¹³ well characterized SSG phases⁷⁻⁹ and SFM domain states^{11,14} are found at $t_n<1.1$ and >1.2 nm, respectively. The transition from SSG to SFM occurs at $t_n\approx 1.1$ nm.¹² Based on this phase diagram, two crossover regimes are still unclear. One is the crossover from SPM to SSG in the very weak interaction limit, and the other one is from SFM to the conventional ferromagnetic state near to the physical percolation threshold. In this paper we focus on the weak interaction limit, as represented by two low coverages, $t_n=0.5$ and 0.7 nm.

The discontinuous magnetic metal-insulator multilayers (DMIM) $[\text{Co}_{80}\text{Fe}_{20}(t_n)/\text{Al}_2\text{O}_3(3\text{ nm})]_{10}$ samples were prepared by focused Xe-ion beam sputtering on glass substrates.¹³ The top view structure of a $\text{Al}_2\text{O}_3(3\text{ nm})/\text{Co}_{80}\text{Fe}_{20}(0.5\text{ nm})/\text{Al}_2\text{O}_3(3\text{ nm})$ trilayer as imaged by transmission electron microscopy (TEM) is shown in Fig. 1. Nearly spherical CoFe particles (dark contrast) with average diameter $d\approx 1.8$ nm are embedded randomly inside the amorphous Al_2O_3 matrix, where the mean distance between two nearest particles is $D\approx 10$ nm. The magnetic properties of the samples are measured by a superconducting quantum interference device (SQUID) magnetometer (Quantum Design, MPMS-5S). In order to compare the experimental results directly, both samples are cut to the same size within an error less than 10%.

The zero-field-cooled (ZFC) and field-cooled (FC) mag-

netic moments, m^{ZFC} and m^{FC} , of the $t_n=0.5$ and 0.7 nm samples are measured in a field $\mu_0 H=10$ mT after cooling the samples in zero field and in $\mu_0 H=10$ mT, respectively. The temperature dependences of m^{ZFC} and m^{FC} are shown in Fig. 2 for the samples with $t_n=0.5$ nm [Fig. 2(a)] and for 0.7 nm [Fig. 2(b)] within the range $2\leq T\leq 100$ K. At difference with experience on DIMMs with higher coverages, where $m^{\text{ZFC}}(T)\approx 0$ and $m^{\text{FC}}(T)\approx \text{const.}$ at very low temperatures,⁸ m^{ZFC} and m^{FC} increase rapidly on cooling to very low T for both samples. Intermediate peaks are observed in $m^{\text{ZFC}}(T)$ at 19 K for the $t_n=0.5$ nm sample and 34 K for $t_n=0.7$ nm. These temperatures roughly determine the blocking (T_b) or the glass temperature (T_g) as will be discussed below. At high temperature Curie laws are observed. Two different regions can be distinguished, if we plot m^{FC} versus T^{-1} as shown in the insets of Figs. 2(a) and 2(b). The broken lines represents the Curie laws, $m^{\text{FC}}(T)=C/T$, for high temperatures, where $C=(5.37\pm 0.03)\times 10^{-7}\text{ Am}^2\text{ K}$ [Fig. 2(a)] and $(3.51\pm 0.01)\times 10^{-6}\text{ Am}^2\text{ K}$ [Fig. 2(b)]. At low temperature one can fit with another straight line (solid line) containing a Curie law with an offset m_0^{FC} , i.e., $m^{\text{FC}}(T)$

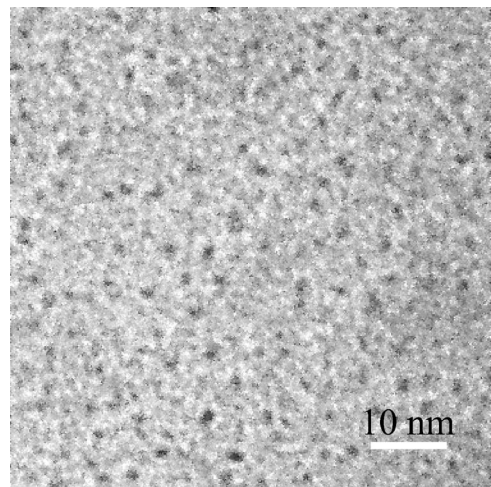


FIG. 1. TEM top view image of an $\text{Al}_2\text{O}_3(3\text{ nm})/\text{Co}_{80}\text{Fe}_{20}(0.5\text{ nm})/\text{Al}_2\text{O}_3(3\text{ nm})$ trilayer being dissolved from a KBr substrate crystal.

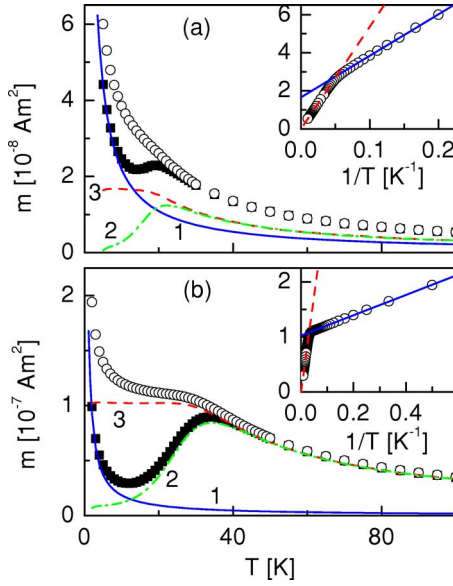


FIG. 2. (Color online) Temperature dependences of m^{ZFC} (solid squares) and m^{FC} (open circles) measured in $\mu_0 H = 10$ mT of $[\text{Co}_{80}\text{Fe}_{20}(t_n)/\text{Al}_2\text{O}_3(3 \text{ nm})]_{10}$ samples with $t_n = 0.5$ (a) and 0.7 nm (b), respectively. The insets show m^{FC} plotted vs T^{-1} , where two straight lines are fitted at high (red dash line) and low (blue solid line) temperatures.

$= C'/T + m_0^{FC}$, where $C' = (2.18 \pm 0.01) \times 10^{-7} \text{ Am}^2 \text{ K}$, $m_0^{FC} = (1.66 \pm 0.01) \times 10^{-8} \text{ Am}^2$ [Fig. 2(a)] and $C' = (1.84 \pm 0.01) \times 10^{-7} \text{ Am}^2 \text{ K}$, $m_0^{FC} = (1.024 \pm 0.001) \times 10^{-7} \text{ Am}^2$ [Fig. 2(b)].

Obviously the magnetization contains two contributions, one of which is paramagnetic down to lowest temperatures, while the other one levels off into a plateau-like contribution at low T . The latter one (shown by the broken lines 3 in the main panels of Fig. 2) becomes apparent after subtracting the paramagnetic Curie function C'/T (solid lines 1) from $m^{FC}(T)$. In addition we show the ZFC curves after subtracting C'/T from $m^{ZFC}(T)$ (dot-dashed lines 2). Now it becomes clear that the high- T Curie characteristics, C'/T , denotes the asymptotic behavior of systems whose particles undergo a blocking or freezing transition at 29 K [Fig. 2(a)] and 44 K [Fig. 2(b)], respectively, where $m^{ZFC}(T)$ (curves 2) and $m^{FC}(T)$ (curves 3) split apart. Based on this simple decomposition, we propose that there are two uncoupled subsystems in the samples: One particle subsystem with N_1 big particles each having a magnetic moment μ_1 , and the other particle subsystem with N_2 small particles each having a magnetic moment μ_2 . These small particles retain their paramagnetic behavior or have a very low blocking temperature, $T_b < 2$ K. The big ones have SPM behavior, but become frozen at low temperatures and thus contribute to m_0^{FC} . Based on the semiclassical model of paramagnetism, we express the asymptotic Curie constants as

$$C = \frac{\mu_0 H (N_1 \mu_1^2 + N_2 \mu_2^2)}{3k_B}, \quad (1)$$

and

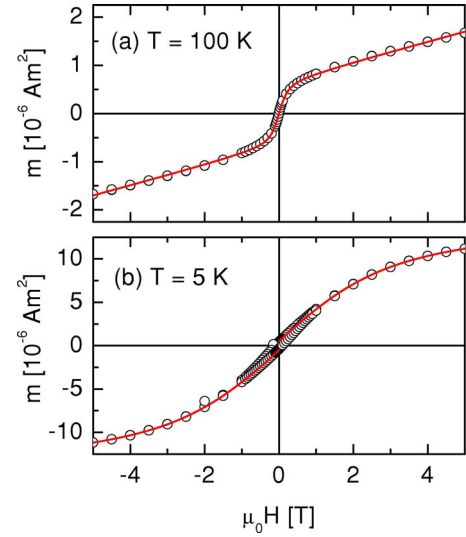


FIG. 3. (Color online) Hysteresis loops $m(\mu_0 H)$ of $[\text{Co}_{80}\text{Fe}_{20}(0.7 \text{ nm})/\text{Al}_2\text{O}_3(3 \text{ nm})]_{10}$ at $T = 100$ K (a) and 5 K (b). The solid lines are the best fits to Eqs. (3) and (4), respectively (see text).

$$C' = \frac{\mu_0 H N_2 \mu_2^2}{3k_B}, \quad (2)$$

where k_B is the Boltzmann constant.

In order to determine the four unknown quantities N_1 , N_2 , μ_1 , and μ_2 , we need other relationships in addition to Eqs. (1) and (2). To this end, we analyze the magnetization curves, $m(\mu_0 H)$, which can be described by Langevin functions, $L(y) = \coth(y) - 1/y$, in the unblocked regime at high enough temperatures, where $y = \mu_1 \mu_0 H / k_B T$. If one chooses T far above T_b (≈ 30 K), the Langevin description is justified for the big particles, while the small particles obey already an asymptotic linear behavior, $m_2 = \chi_2 V_2 H$, where χ_2 and V_2 are the dc susceptibility and the volume of the small particle subsystem. Then the total moment reads

$$m = N_1 \mu_1 L\left(\frac{\mu_1 \mu_0 H}{k_B T}\right) + \chi_2 V_2 H. \quad (3)$$

On the other hand, at low temperatures the big particle subsystem becomes saturated at high field, $|m_1| = m_{s1}$, where m_{s1} is the saturated magnetic moment of the big particles. Its contribution is independent of $\mu_0 H$, but depends on the sign of $\mu_0 H$. Hence, at low temperatures and high fields one has

$$m = m_{s1} \frac{H}{|H|} + N_2 \mu_2 L\left(\frac{\mu_2 \mu_0 H}{k_B T}\right). \quad (4)$$

Figure 3 shows the $m(\mu_0 H)$ curves for the $t_n = 0.7$ nm sample at $T = 100$ K [Fig. 3(a)] and at 5 K [Fig. 3(b)]. The solid lines are the best fits to Eq. (3) in Fig. 3(a) and to Eq. (4) in Fig. 3(b). Note that only data at $|\mu_0 H| \geq 1.5$ T, i.e., outside the low-field hysteresis, are used to fit Eq. (4) in Fig. 3(b). One obtains the parameters $N_1 = (4.46 \pm 0.17) \times 10^{13}$ and $\mu_1 = (1619 \pm 68) \mu_B$ for the big particles, and N_2

$= (2.512 \pm 0.004) \times 10^{17}$ and $\mu_2 = (6.03 \pm 0.02) \mu_B$ for the small particles. Additionally, $\chi_2 V_2 = (2.63 \pm 0.02) \times 10^{-13}$ and $m_{s1} = (5.2 \pm 0.3) \times 10^{-7} \text{ Am}^2$. Substituting these values into Eqs. (1) and (2), one obtains $C = (2.6 \pm 0.3) \times 10^{-6} \text{ Am}^2 \text{ K}$ and $C' = (1.88 \pm 0.02) \times 10^{-7} \text{ Am}^2 \text{ K}$. Comparing to the experimental results from Fig. 2(b), one finds that C' is nearly the same within errors, while C is 31% smaller. The latter deviation is probably due to the finite size distribution of the big particles, which is neglected in the present analysis and enters with different weights into Eqs. (1) and (3), respectively. Under the assumption of an effective atomic moment of the $\text{Co}_{80}\text{Fe}_{20}$ alloy, $\mu_{\text{CoFe}} \approx 1.9 \mu_B$,¹⁵ the average number of atoms per particles is $n_1 \approx 850$ and $n_2 \approx 3$. Hence, a bimodal distribution of nanoparticles (diameters $d_1 \approx 2.6 \text{ nm}$ when assuming the lattice parameters of bulk fcc $\text{Co}_{80}\text{Fe}_{20}$) and “molecules” $\text{Co}_{3-n}\text{Fe}_n$ ($n=0-3$) is encountered.

The same analysis performed on the $m(\mu_0 H)$ curves of the $t_n=0.5 \text{ nm}$ sample (not shown) yields $N_1 = (4.31 \pm 0.14) \times 10^{13}$, $\mu_1 = (561 \pm 12) \mu_B$, $d_1 \approx 1.8 \text{ nm}$, and $N_2 = (2.791 \pm 0.001) \times 10^{17}$, $\mu_2 = (6.04 \pm 0.01) \mu_B$. Remarkably, d_1 of the TEM estimate (Fig. 1) is confirmed by magnetometry. Further, as expected,^{9,13} the magnetic moment of the big particles, μ_1 , decreases as the nominal thickness t_n decreases, whereas μ_2 remains constant. From the latter value one can conclude that the small particles are indeed clusters containing only few atoms which cannot be observed in TEM. One might even envisage isolated single Co or Fe atoms or ions (Co^{2+} and Fe^{2+} or Fe^{3+}) bonded to the amorphous oxide environment with magnetic moments in the order $\mu_2 \approx 6 \mu_B$ as expected for the $^4F_{9/2}$, 5D_4 ($^6S_{5/2}$) ionic ground states.¹⁶ A similar system, $\text{Al}_2\text{O}_3/\text{Co}(t_n)/\text{Al}_2\text{O}_3$ trilayers, was studied by Maurice *et al.* with TEM and extended x-ray absorption fine structure (EXAFS).¹⁷ The main particle sizes estimated from TEM were much larger than the sizes calculated from EXAFS spectra for $t_n \leq 0.7 \text{ nm}$ (61% and 47% larger for $t_n = 0.4$ and 0.7 nm , respectively). They assumed that TEM misses an appreciable fraction of very small particles, which are also suggested by Monte Carlo simulations on the growth processes.¹⁸ This is confirmed by the present investigation, where these TEM-undetectable “dark” particles have a large contribution to the magnetic moment, which offers the chance to “see” them in detail by magnetic measurements. Future experiments, e.g., by using Mössbauer spectroscopy of ^{57}Fe , will have to unravel the presently unsolved question, if single ions like Fe^{3+} ($m=5.9 \mu_B$) or—less probably—metallic molecules $\text{Co}_{3-n}\text{Fe}_n$ (e.g., $m=8-9 \mu_B$ for $n=1-2$)¹⁹ are at the origin of the newly detected “dark” particles.

Within errors N_1 remains constant while t_n increases, i.e., the number densities of the big particles is independent of t_n . This is an evidence of a Volmer-Weber-type growth mode in our $\text{CoFe}/\text{Al}_2\text{O}_3$ system.^{9,13} With increasing t_n , starting from a constant concentration of nuclei, the big particles grow. Because of the large distance between particles ($D \approx 10 \text{ nm}$), the particles do not touch each other during growth at low concentration. Hence the density of the big particles does practically not change. A similar kind of growth mechanism has widely been observed for metals grown on oxide surfaces.^{17,18,20} As a result of Volmer-Weber-type growth, these ultrasmall particles might refer to the

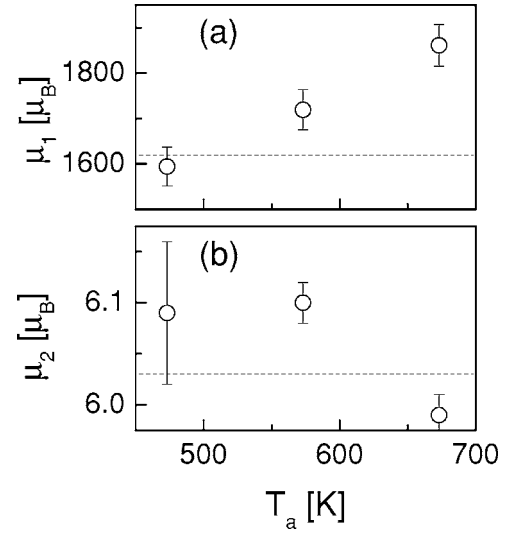


FIG. 4. Dependences of μ_1 (a) and μ_2 (b) on the annealing temperature T_a for the sample $[\text{Co}_{80}\text{Fe}_{20}(0.7 \text{ nm})/\text{Al}_2\text{O}_3(3 \text{ nm})]_{10}$. The dashed lines indicate the values before annealing.

metal atoms being deposited on the oxide surface, but do not have enough time to move to the nucleation sites, where the large particles grow.

A slight increase of the number of small particles N_2 by about 10% is observed when decreasing t_n from 0.7 to 0.5 nm. This might be due to the increase of the average diffusion paths of the ultrasmall particles and a decreasing impingement at the big particles owing to their smaller cross section.

Annealing has been carried out in order to gain deeper insight into the growing process. The $t_n=0.7 \text{ nm}$ sample was annealed in nitrogen atmosphere for 10^4 s at $T_a=473$, 573 and 673 K, respectively. After each annealing step, m^{FC} versus T and m versus H were measured and analyzed as previously (see above). Figures 4(a) and 4(b) show the dependences of μ_1 and μ_2 on T_a , respectively. As expected, μ_1 increases by approximately 10% as T_a increases, while μ_2 remains virtually constant. Obviously at higher temperature enhanced diffusion of the ultrasmall particles is activated, which helps the large particles growing. On the other hand, the ultrasmall particles do obviously not aggregate to become larger.

The dipole-dipole interparticle interaction energy between adjacent big particles can be estimated from the formula $E_{d-d}/k_B = (\mu_0/4\pi k_B) \mu_1^2/D^3$. With $D=10 \text{ nm}$, $\mu_1=561 \mu_B$ for the $t_n=0.5 \text{ nm}$ sample one obtains $E_{d-d}/k_B \approx 0.2 \text{ K}$. Considering twelve nearest neighbors for each particle, the dipolar interaction energy yields $E_{d-d}/k_B \approx 2.4 \text{ K}$ which is much smaller than $T_b \approx 29 \text{ K}$ [Fig. 2(a)]. Similarly, we estimate the dipolar interaction energy for the $t_n=0.7 \text{ nm}$ sample to be $\approx 20 \text{ K}$, which is in the order of T_g (see below) $\approx 34 \text{ K}$ [Fig. 2(b)]. Obviously, quite strong interparticle interactions exist in this sample, which might give rise to a collective state rather than individual SPM behavior being more favorable in the 0.5 sample.

In order to check this conjecture, a dynamic study is performed with the aim to clarify our nanoparticle systems to be

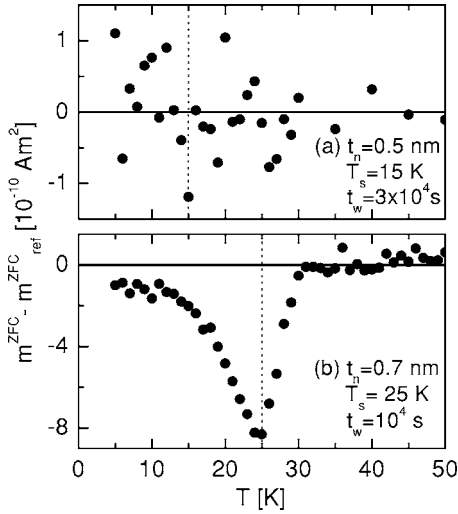


FIG. 5. Difference curves of m^{ZFC} with and without intermittent stop at T_s for $[\text{Co}_{80}\text{Fe}_{20}(t_n)/\text{Al}_2\text{O}_3(3 \text{ nm})]_{10}$ samples with $t_n=0.5$ (a) and 0.7 nm (b). Here m^{ZFC} is measured in 10 mT after ZFC from 100 to 5 K with a stop at $T_s=15$ K for 3×10^4 s (a) and $T_s=25$ K for 10^4 s (b) (vertical broken lines), while the reference m_{ref}^{ZFC} is measured in the same way, but without stops.

either blocked SPM or collective SSG. It is well known that both of these states have very slow dynamics, which are very difficult to distinguish from each other. However, Sasaki *et al.*²¹ demonstrated that the memory effect found in the ZFC magnetization is an unequivocal signature of SSG behavior. In the SPM case, no memory is imprinted during a ZFC process below T_b , since the occupation probabilities of spin up and spin down states are always equal to 0.5 (two-state model). However, in the SSG case the sizes of droplets are growing even during the ZFC process as time elapses in the collective SSG state below T_g . This gives rise to a well-defined memory effect.

Memory effects are studied on both samples being cooled in zero magnetic field from high temperature with or without an intermittent stop at $T_s < T_b$ (or T_g) for a waiting time t_w , respectively. $m^{ZFC}(T)$ is recorded during subsequent heating in a field of 10 mT. The difference curves between $m^{ZFC}(T)$ with and without intermittent stop are plotted in Fig. 5. A memory effect shown as a dip at $T \approx T_s = 25$ K is clearly observed for the 0.7 nm sample [Fig. 5(b)]. Hence we conclude that this sample is a SSG system. However, in Fig. 5(a) no ZFC memory effect is found beyond noise for the 0.5 nm sample, which most probably implies a noncollective SPM blocking state. Obviously the crossover from SPM to SSG occurs at $0.5 < t_n < 0.7$ nm.

The SSG nature of the $t_n=0.7$ nm sample is corroborated by ac susceptibility measurements as shown in Fig. 6. Here χ' versus T is measured after ZFC to 5 K with an amplitude $\mu_0 h_{ac}=0.4$ mT and frequencies $10^{-1} \leq f \leq 10^3$ Hz. The peaks, $T_m(f)$, are observed to shift towards a finite glass temperature T_g as f decreases. As observed for other SSG-type DMIMs,⁸ the critical behavior of the average relaxation time, $\tau = (2\pi f)^{-1}(T_m) = \tau_0 \varepsilon^{-z\nu}$, is obtained from the best fit shown in the inset to Fig. 6, where $\varepsilon = T_m/T_g - 1$ is the reduced temperature with $T_g = 31.9 \pm 1.4$ K. The relaxation time for an

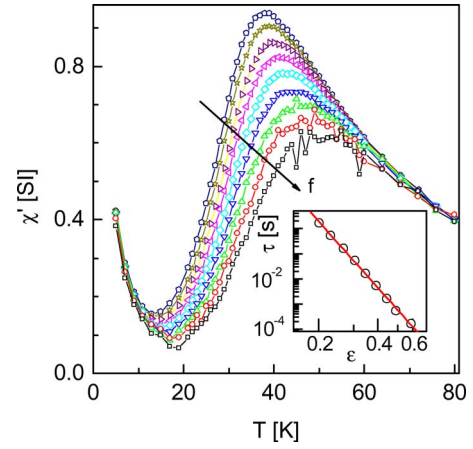


FIG. 6. (Color online) Temperature dependence of the real part of the ac susceptibility χ' of $[\text{Co}_{80}\text{Fe}_{20}(0.7 \text{ nm})/\text{Al}_2\text{O}_3(3 \text{ nm})]_{10}$ measured at an ac amplitude $\mu_0 h_{ac}=0.4$ mT with frequencies $f=0.1, 0.3, 1, 3, 10, 30, 100, 300$, and 1000 Hz, respectively. The inset shows a double logarithmic plot of τ vs ε (open circles) and the best fit to a critical power law (solid line).

individual particle $\tau_0 = (1.2 \pm 0.5) \times 10^{-6}$ s and the critical exponent $z\nu = 8.9 \pm 1.1$ are similar to the values obtained for a SSG with $t_n=0.9$ nm.⁹

The temperature dependence of the ac susceptibility of the $t_n=0.5$ nm sample has also been measured (not shown). Analysis of the peak position of χ' versus T yields the fitting parameters $T_g = 23.4 \pm 1.1$ K, $\tau_0 = (4.2 \pm 2.6) \times 10^{-6}$ s and $z\nu = 6.0 \pm 1.5$ when fitting to an algebraic law, $\tau = \tau_0 \varepsilon^{-z\nu}$. While the values of $z\nu$ and T_g still seem reasonable, the fitting parameter $\tau_0(t_n=0.5 \text{ nm})$ being larger than $\tau_0(t_n=0.7 \text{ nm})$ contradicts expectation, where the smaller particles should relax faster than the larger ones. Further, the $\tau(T_m)$ data of the $t_n=0.5$ nm system better comply with an Arrhenius law, $\tau = \tau^* \exp(E/k_B T)$, for weakly interacting magnetic particles with modified relaxation time τ^* and activation energy barrier E .⁴ First, $\log_{10} \tau^* = -17.1 \pm 0.8$ confirms the predicted value, $\log_{10} \tau^* = -17$ to -18 . Second, $E/k_B = 448 \pm 23$ K seems to reveal the expected enhancement due to the dipolar interaction,⁴ since an energy barrier $KV/k_B \approx 150$ K is expected for isolated particles possessing bulk Co anisotropy. Together with the obvious lack of memory effects, we believe that the $t_n=0.5$ nm sample does not represent a generic (super)spin glass system, but rather marks the crossover into the regime of dipolarly interacting SPM nanoparticles. It should be noticed that a tentative Arrhenius fit of the $\tau(T_m)$ data of the $t_n=0.7$ nm system fails to show the expected increase of the energy barrier in proportion to the particle volume when assuming the same interaction-based increase as in the case $t_n=0.5$ nm. Instead of $E/k_B \approx 1300$ K the fit merely yields $E/k_B \approx 700$ K, which clearly disproves a possible description as a dipolar interaction-modified nanoparticle system. Needless to say that the very existence of the memory effect in this case is much more convincing of cooperative glassy behavior than any fit of $\tau(T_m)$ selected out of the wide spectrum of relaxation times.

In conclusion, Volmer-Weber-type growth of heterogeneously nucleated nanoparticles with average interparticle

distance $D \approx 10$ nm has been verified in discontinuous multilayers $[\text{Co}_{80}\text{Fe}_{20}(t_n)/\text{Al}_2\text{O}_3(3\text{ nm})]_{10}$ for low coverages, $t_n = 0.5$ and 0.7 nm. Magnetization studies evidence that the nanoparticles with diameters $d_1 \approx 1.8$ and 2.6 nm, respectively, are surrounded by myriads of unattached CoFe molecules (concentration ratio $10^4:1$). We cannot exclude that tunneling exchange between the large particles^{7,22} is mediated by these ultrasmall ones. The nanoparticle systems experience a size controlled crossover from SPM to SSG behavior as evidenced by independent blocking for $t_n = 0.5$ nm,

but spin-glass-like freezing with a ZFC memory effect for $t_n = 0.7$ nm.

ACKNOWLEDGMENTS

Thanks are due to S. Stappert for providing the transmission electron micrographs and to the DFG (KL306/37-1 and Graduate School "Structure and dynamics of heterogeneous systems") for financial support.

*Electronic address: chen@kleemann.uni-duisburg.de

¹L. Néel, Ann. Geophys. (C.N.R.S.) **5**, 99 (1949).

²W. F. Brown, Jr., Phys. Rev. **130**, 1677 (1963).

³S. Shtrikmann and E. P. Wohlfarth, Phys. Lett. **85A**, 467 (1981).

⁴J. L. Dormann, D. Fiorani, and E. Tronc, Adv. Chem. Phys. **98**, 283 (1997).

⁵J. L. Dormann, R. Cherkaoui, L. Spinu, M. Nogués, F. Lucari, F. D'Orazio, D. Fiorani, A. Garcia, E. Tronc, and J. P. Jolivet, J. Magn. Magn. Mater. **187**, L139 (1998).

⁶C. Djurberg, P. Svedlindh, P. Nordblad, M. F. Hansen, F. Bodker, and S. Morup, Phys. Rev. Lett. **79**, 5154 (1997).

⁷W. Kleemann, O. Petravic, Ch. Binek, G. N. Kakazei, Yu. G. Pogorelov, J. B. Sousa, S. Cardoso, and P. P. Freitas, Phys. Rev. B **63**, 134423 (2001).

⁸S. Sahoo, O. Petravic, Ch. Binek, W. Kleemann, J. B. Sousa, S. Cardoso, and P. P. Freitas, Phys. Rev. B **65**, 134406 (2002).

⁹S. Sahoo, O. Petravic, W. Kleemann, S. Stappert, G. Dumpich, P. Nordblad, S. Cardoso, and P. P. Freitas, Appl. Phys. Lett. **82**, 4116 (2003).

¹⁰U. Bovensiepen, P. Pouloupoulos, W. Platow, M. Farle, and K. Baberschke, J. Magn. Magn. Mater. **192**, L386 (1999).

¹¹X. Chen, O. Sichel Schmidt, W. Kleemann, O. Petravic, Ch. Binek, J. B. Sousa, S. Cardoso, and P. P. Freitas, Phys. Rev. Lett. **89**, 137203 (2002).

¹²X. Chen, S. Sahoo, W. Kleemann, S. Cardoso, and P. P. Freitas, Phys. Rev. B **70**, 172411 (2004).

¹³G. N. Kakazei, Yu. G. Pogorelov, A. M. L. Lopes, J. B. Sousa, S.

Cardoso, P. P. Freitas, M. M. Pereira de Azevedo, and E. Snoeck, J. Appl. Phys. **90**, 4044 (2001).

¹⁴X. Chen, W. Kleemann, O. Petravic, O. Sichel Schmidt, S. Cardoso, and P. P. Freitas, Phys. Rev. B **68**, 054433 (2003).

¹⁵R. H. Victora and L. M. Falicov, Phys. Rev. B **30**, 259 (1984).

¹⁶S. Blundell, *Magnetism in Condensed Matter* (Oxford University Press, New York, 2001), p. 49.

¹⁷J. L. Maurice, J. Briático, J. Carrey, F. Petroff, L. F. Schelp, and A. Vaurès, Philos. Mag. A **79**, 2921 (1999).

¹⁸J. Briático, J. L. Maurice, J. Carrey, D. Imhoff, F. Petroff, and A. Vaurès, Eur. Phys. J. D **9**, 517 (1999).

¹⁹G. Mpourmpakis, G. E. Froudakis, A. N. Andriotis, and M. Me-non, Phys. Rev. B **72**, 104417 (2005).

²⁰C. Morawe and H. Zabel, J. Appl. Phys. **77**, 1969 (1995); U. Diebold, J. Pan, and T. E. Madey, Surf. Sci. **331-333**, 845 (1995); N. M. Dempsey, L. Ranno, D. Givord, J. Gonzalo, R. Serna, G. T. Fei, A. K. Petford-Long, R. C. Doole, and D. E. Hole, J. Appl. Phys. **90**, 6268 (2001); J.-P. Barnes, A. K. Petford-Long, R. C. Doole, R. Serna, J. Gonzalo, A. Suárez-García, C. N. Afonso, and D. Hole, Nanotechnology **13**, 465 (2002).

²¹M. Sasaki, P. E. Jönsson, H. Takayama, and H. Mamiya, Phys. Rev. B **71**, 104405 (2005).

²²M. R. Scheinfein, K. E. Schmidt, K. R. Heim, and G. G. Hem-bree, Phys. Rev. Lett. **76**, 1541 (1996); V. N. Kondratyev and H. O. Lutz, *ibid.* **81**, 4508 (1998); Eur. Phys. J. D **9**, 483 (1999).